2018

Observation-Driven Estimation of the Spatial Variability of 20th Century Sea Level Rise

B. D. Hamlington
Old Dominion University, bhamling@odu.edu

A. Burgos
Old Dominion University

P. R. Thompson

F. W. Landerer

C. G. Piecuch

See next page for additional authors

Original Publication Citation

Hamlington, B. D., Burgos, A., Thompson, P. R., Landerer, F. W., Piecuch, C. G., Adhikari, S., . . . Ivins, E. R. (2018). Observation-driven estimation of the spatial variability of 20th century sea level rise. *Journal of Geophysical Research: Oceans, 123*(3), 2129-2140. doi:10.1002/2017JC013486

AGU PUBLICATIONS

JGR

Journal of Geophysical Research: Oceans

RESEARCH ARTICLE

10.1002/2017JC013486

Observation-Driven Estimation of the Spatial Variability of 20th Century Sea Level Rise

B. D. Hamlington[1], A. Burgos[1], P. R. Thompson[2], F. W. Landerer[3], C. G. Piecuch[4], S. Adhikari[3], L. Caron[3], J. T. Reager[3], and E. R. Ivins[3]

[1]Department of Ocean, Earth and Atmospheric Sciences, Old Dominion University, Norfolk, VA, USA, [2]Department of Oceanography, University of Hawai'i at Manoa, Honolulu, HI, USA, [3]Jet Propulsion Laboratory, California Institute of Technology, CA, USA, [4]Atmospheric and Environmental Research, Inc, Lexington, MA, USA

Abstract Over the past two decades, sea level measurements made by satellites have given clear indications of both global and regional sea level rise. Numerous studies have sought to leverage the modern satellite record and available historic sea level data provided by tide gauges to estimate past sea level rise, leading to several estimates for the 20th century trend in global mean sea level in the range between 1 and 2 mm/yr. On regional scales, few attempts have been made to estimate trends over the same time period. This is due largely to the inhomogeneity and quality of the tide gauge network through the 20th century, which render commonly used reconstruction techniques inadequate. Here, a new approach is adopted, integrating data from a select set of tide gauges with prior estimates of spatial structure based on historical sea level forcing information from the major contributing processes over the past century. The resulting map of 20th century regional sea level rise is optimized to agree with the tide gauge-measured trends, and provides an indication of the likely contributions of different sources to regional patterns. Of equal importance, this study demonstrates the sensitivities of this regional trend map to current knowledge and uncertainty of the contributing processes.

Key Points:
- Regional sea level trends are computed using tide gauges and estimates of the structure of the processes contributing to sea level change
- The regional sea level trends are optimized to agree with the tide gauges, providing an indication of the contribution of different sources
- This study demonstrates the sensitivities of this regional trend map to current knowledge and uncertainty of the contributing processes

Supporting Information:
- Supporting Information S1

Correspondence to:
B. D. Hamlington,
bhamling@odu.edu

Citation:
Hamlington, B. D., Burgos, A., Thompson, P. R., Landerer, F. W., Piecuch, C. G., Adhikari, S., et al. (2018). Observation-driven estimation of the spatial variability of 20th century sea level rise. *Journal of Geophysical Research: Oceans*, *123*, 2129–2140. https://doi.org/10.1002/2017JC013486

Received 22 SEP 2017
Accepted 22 FEB 2018
Accepted article online 15 MAR 2018
Published online 24 MAR 2018

1. Introduction

At many locations across the globe, planning efforts for impending sea level rise are already underway. While assessments of the global rate of sea level change provide an important indicator of the changing climate, the salient information for planning efforts is how sea level varies regionally. Over the past two decades, sea level has been measured continuously and with near-global coverage by satellite altimeters, leading to clear indications of both global and regional sea level rise (Church et al., 2013). Unfortunately, it is a challenge to extract useful information regarding long-term sea level changes over the past century using altimeter-measured rates, as they are heavily influenced by interannual- to decadal-scale variability (e.g., Boening et al., 2012; Cazenave et al., 2012; Fasullo et al., 2013; Hamlington et al., 2016a). On global scales, numerous efforts have been made to leverage the modern satellite record and available historic sea level data provided by tide gauges to estimate past sea level rise, leading to estimates of the 20th century trend in global mean sea level (GMSL) ranging from 1.1 mm/yr to 1.9 mm/yr (Church & White, 2006, 2011; Church et al. 2004; Dangendorf et al., 2017; Jevrejeva et al., 2014; Hay et al., 2015; Ray & Douglas, 2011; Thompson et al., 2016). On regional scales, there have been fewer attempts to constrain trends over the same time period, reflecting the challenges presented by the available measurements of past sea level (Hay et al., 2017; Wenzel & Schröter, 2014).

Since the beginning of the 19th century, tide gauges have provided measurements of relative sea level rise at specific locations across the globe. While generally providing long records, their usefulness is limited for a variety of reasons. Perhaps most problematic is the inconsistency of sampling both in space and time. There is a strong hemispheric bias, with the majority of gauges located around heavily populated areas in the northern hemisphere. The record length of the tide gauges varies dramatically, with only a relatively small subset providing measurements for the majority of the 20th century. Even when the records are long, gaps in the records on the order of several years often exist. In terms of the measurements they provide, tide gauges also measure *relative* sea level rise, specifically vertical displacement of the sea surface relative to the land upon which the tide gauge is located. This presents a confounding issue because for many tide gauges, it is difficult or impossible to fully correct for vertical land motion. Typically, relative sea level trends associated with glacial isostatic

adjustment (GIA) are modeled and subsequently removed from the tide gauge records (e.g., Church & White, 2006; 2011 Church et al., 2004; Ray & Douglas, 2011; Thompson et al., 2016). Predictions of existing GIA models, however, differ significantly, which can impact trends estimated from tide gauge data over long timescales. Beyond GIA, there is potentially other vertical land motion signals that are non-stationary and highly uncertain prior to the advent Global Positioning System (GPS) measurements over the last two decades. Recent studies have corrected tide gauge records for vertical land motion using GPS measurements (Dangendorf et al., 2017; Hamlington et al., 2016a; Santamaría-Gómez et al., 2012; Wöppelmann & Marcos, 2016), but many tide gauges have no collocated GPS observation and questions remain regarding the applicability of a trend measured over one or two decades to longer timescales to tide gauges in general.

To overcome the sampling challenges presented by the tide gauge network, a variety of methods have been proposed in recent years to combine improved spatial information from modern data records and models with the longer historic records (Church & White, 2006, 2011; Church et al. 2004; Dangendorf et al., 2017; Hamlington et al., 2011; Hay et al., 2015; Ray & Douglas, 2011; Thompson et al., 2016). Typically, these efforts have focused on the reconstruction of GMSL back through time with few published attempts at reproducing the spatial pattern of sea level trends during the majority of the 20th century. Even after producing a 20th century regional trend map, there are questions regarding how to validate or "confirm" the resulting trend maps, as the only available observations of sea level during the 20th century come from the tide gauges. The applied techniques for reconstructing sea level are also often necessarily complex, making it difficult to assess sensitivities and understand the implications of assumptions that are made.

Here, we seek to simplify the process, building off the efforts of Thompson et al. (2016) to constrain the rate of GMSL rise and extending the technique to estimate the spatial variability in 20th century sea level rise. As mentioned above, the main challenges in using tide gauges to estimate long-term regional trends are poor sampling in space, inconsistent sampling in time, and unresolved vertical land motion that impacts the trend. First, through careful tide gauge selection, we seek to reduce the impact of inconsistent sampling in time and unresolved vertical land motion. We only select gauges with long and complete records during the 20th century ($>$70% complete) and for which there is no documented evidence of significant non-GIA vertical land motion, leading to a set of 15 gauges (list provided in supporting information Table S1 and shown in figures). It should be noted that although the editing criteria was intentionally strict and the small set of remaining gauges is not unexpected, the results obtained here are potentially sensitive to this particular set of tide gauges. Without the ability to find more gauges meeting this criteria, this paper is presented with the caveat that the results could differ given the availability of more tide gauges. The mean linear trend of these 15 gauges is 1.69 mm/yr with a standard deviation of 0.54 mm/yr. Next, after obtaining this set of tide gauges, we attempt to account for the dominant processes that lead to spatial variability in these gauges on long timescales. In other words, we attempt to account for and explain the sources that are contributing to the standard deviation of 0.54 mm/yr in these long-term sea level trends. The methodological focus is on relative sea level trends that are estimated after removing the effect of GIA, but this work does highlight the impact of the choice of GIA correction on the resulting global and regional trends. Beyond GIA, we attempt to account for the dominant processes that could lead to the spatial variability in these gauges on 100 year timescales, based on: 1) ocean dynamics, 2) the self-attraction/loading (SAL) patterns of ice melt, 3) SAL of terrestrial groundwater depletion, and 4) SAL of water impoundment on land. In Thompson et al. (2016), ice melt was accounted for using melt fingerprints generated using data from the GRACE satellites, and ocean dynamics was accounted for using empirical orthogonal functions (EOFs) determined from the Coupled Model Intercomparison Project 5 (CMIP5) dynamic sea level trends. By generating random combinations of these patterns that reduced the spread in trends of the 15 GIA-corrected tide gauges and are consistent with published estimates of 20th century ice melt, it was shown that the true rate of GMSL rise in the 20th century is underestimated at the 15 tide gauge locations by 0.08 mm/yr. By modifying this procedure and expanding it to account for more of the contributors to regional sea level rise, it is possible to generate 20th century trend maps under the same constraints and using the same assumptions as in Thompson et al. (2016).

2. Equation for Regional Sea Level Trends

To estimate the 20th century sea level trend (SLT) at each location across the globe, we consider the following equation for the long-term trend as measured by a tide gauge minimally impacted by non-GIA vertical land motion:

$$SLT(r) = GIA(r) + IB(r) + IM(r) + OD(r) + GW(r) + WI(r) + GC \quad (1)$$

where GIA is the relative sea level trend contribution of the glacial isostatic adjustment (combining both the vertical land motion and geoid effects of GIA), IB is the contribution from long-term trends in atmospheric loading at each tide gauge, IM is the regionally varying trend associated with the self-attraction/loading patterns of ice melt, OD is the regionally varying trend associated with changes in ocean dynamics and the phasing of internal variability, GW is the regional pattern of sea level change resulting from groundwater depletion, WI is the regional pattern associated with water impoundment in reservoirs and dams, and GC is a globally uniform trend that includes the contribution of thermal expansion. Note that all the components of the equation other than GC varying spatially, denoted by the (r) for each contributor. It should be noted that while we describe the term GC as dominantly associated with thermal expansion, other contributors to 20th century GMSL that are not considered directly in our technique or incorrectly accounted for in our randomization procedure will also be included in GC. Further discussion on this term is provided in the remainder of the paper. Here, we are interested in generating a 20th century regional trend map associated with the last five terms on the right hand side of equation (1), but also attempt to understand the uncertainty that arises when trying to account for the other terms.

Trends associated with the inverted barometer (IB) effect using the mean of three 20th century atmospheric pressure data sets are first removed from the set of 15 tide gauges, following the results and discussion from Piecuch et al. (2016). To account for and remove the trends associated with GIA, we generate new solutions using the method from Caron et al. (2017), a Bayesian approach that provides expected GIA estimates and uncertainties thereof. In our case, the solid Earth model features a mantle with Maxwell rheology, and the reference ice history model is the ANU (Lambeck et al., 2010, 2014) model in the Nothern Hemisphere, the Ivins et al. (2013) model in Patagonia, and the Ivins and James (2004) model in Antarctica. The inversion is constrained by 11,451 relative sea level records and 459 GPS stations. Fingerprints of relative sea level rise associated with mass redistribution over the Earth's surface are computed following the technique of Adhikari et al. (2016), and used to account for the regional trend variability associated with IM, GW and WI. In total, nine of these fingerprints are used – five associated with glaciers, two associated with the ice sheets, and one each for groundwater withdrawal and water impoundment.

To account for the regional variability of the trends associated with changes in OD, a sea level reconstruction of climate variability during the 20th century is used. As demonstrated in Calafat et al. (2014), commonly used reconstruction techniques have difficulty in accounting for the long-term global trend and accurately representing the variability about this trend. Specifically, when including a spatially constant basis function to account for the long-term trend in global mean sea level, the ability to describe the variability about the long-term trend – both globally and regionally – is dramatically reduced. By applying the conclusions of that study regarding the inclusion of a spatially constant basis function and following the technique of Hamlington et al. (2012), a sea level reconstruction is created specifically focused on reconstructing the variability about the long-term trend from 1900 to 2014. No attempt is made to account for the long-term trend in global mean sea level, and instead patterns describing the fluctuations about the trend associated with internal variability are reproduced back to 1900. Specifically, the global mean of the altimeter record is removed prior to computing cyclostationary empirical orthogonal basis functions (CSEOFs) for the reconstruction. The resulting CSEOF decomposition does not return a basis function that describes the global trend in the altimeter GMSL, and following the discussion in Calafat et al. (2014), we do not include a spatially constant basis function to capture this trend. The focus here is on accurately representing the variability about this trend. It should be noted that – as with any reconstruction – it can be difficult to ascertain the full extent of the variability that is being reconstructed, and we leave open the possibility of biasing unaccounted-for variability in ways that are difficult to estimate. As described in Hamlington et al. (2012), representing the variability about the trend with tide gauge data alone is a challenge given the poor sampling in the first half of the 20th century. As a result, past sea surface temperature observations are used to supplement the reconstruction. Specifically, we use an ensemble of one thousand Extended Reconstructed Sea Surface Temperature (ERSST) v4 data sets (Huang et al., 2015). This reconstructed SST data set is a gridded global monthly data set derived from the ICOADS but with enhanced spatial completeness using statistical methods. A separate sea level reconstruction is created for each data set in the ensemble, allowing us to capture the uncertainty arising from both the sea level and sea surface temperature portions of the reconstruction. Further details on this technique can be found in Hamlington et al. (2012), with the

main difference being the exclusion of the long-term trend in global mean sea level. In using this reconstruction to account for the trends associated with OD, we assume that spatial differences in long-term dynamic trends occur primarily due to phasing of decadal and multidecadal climate modes. We subsample the sea level reconstruction at the tide gauge locations, and – using only the time span actually covered by the tide gauge record – compute the trends represented by OD in equation (1) above. As a second, alternative method of accounting for the OD-related trends, we also implement EOFs of the CMIP5 dynamic trends as in Thompson et al. (2016). It should be noted, however, that since the models do not capture the phasing of internal variability, the trends cannot be computed over the specific time period that the tide gauges actually cover. Correctly accounting for and removing the OD trend associated with the time period actually covered by the tide gauge record has potentially important implications for the results in this study.

3. Randomization Procedure

After the trend associated with the IB effect is removed, combinations of GIA trends, ocean dynamic trends, and amplitudes of the mass redistribution fingerprints are randomly generated. These combinations are drawn according to constraints placed on each contributor. For the GIA corrections, values for each gauge are drawn from a multivariate normal distribution centered on the expected value from the Bayesian framework and accounting for the covariance between the GIA signal at the 15 locations (Caron et al., 2018). The distributions from which the amplitudes of the fingerprints are drawn are formed based on the state of knowledge in recent literature as described in Thompson et al. (2016). The discussion of the amplitude selection is summarized briefly here, and the interested reader is referred to Thompson et al. (2016) for further details. Recent synthesis studies of twentieth century cryospheric observations estimate that the total amount of glacier melt outside of Greeland and Antartica has 90% confidence interval of (0.47 0.61) mm/yr (Church et al. 2013; Vaughan et al., 2013). Amplitudes for the five glacier fingerprints are thus constrained to sum to the same confidence interval. Melt from Greenland glaciers has a 90% confidence interval of (0.1 0.19) mm/yr, while melt from the Greenland ice sheet is much more uncertain with model estimates suggesting a range of $+/-$ 0.25 mm/yr (Gregory et al., 2013). Based on these estimates, the amplitude of the Greenland fingerprint is modeled as the sum of the randomly slected Greenland glacier melt rate plus a random number representing the ice sheet melt from a distribution with a 90% confidence interval of $+/-$ 0.25 mm/yr. Finally, Gregory et al. (2013) and Huybrechts et al. (2011) loosely constrain the Antarctic melt rate during the twentieth century to be between -0.2 mm/yr and 0.5 mm/yr. Amplitudes for the Antarctic fingerprint are thus chosen from a 90% probability range of (-0.2 0.5) mm/yr. Based on geodetic observations, the total amount of melt from all sources is constrained to be less than 1 mm/yr, which is enforced once amplitudes for each fingerprint are generated (Mitrovica et al., 2006). Thompson et al. (2016) did not incorporate fingerprints for GW ad WI. The amplitudes for these contributions were drawn from normal distributions with means of 0.17 mm/yr (Wada et al., 2012) and -0.16 mm/yr (Lehner et al., 2011). and standard deviations of 0.07 mm/yr and 0.1 mm/yr, respectively. It should be noted that the WI fingerprint used here accounts for only 60% of the global reservoir storage, leading to a reduced estimate of the contribution of reservoirs to GMSL over the past century. Furthermore, both of these contributions are known to change over the course of the 20th century, although here we work only with the 20th century rate contribution and ignore the variations about this long-term trend or any acceleration. Finally, it is assumed in this randomization procedure that the generated amplitudes and the associated contributions of each fingerprint are independent, which in reality is not the case. The dependence of these contributions is not explicitly accounted for and can be viewed as a shortcoming of this analysis. By retaining only combinations that reduce the spread of the trends in the tide gauges (see below), however, it is unlikely that a set of amplitudes will be generated that are very inconsistent. Regardless, this potential limitation should be kept in mind in the results presented here.

As mentioned above, two different cases are tested resulting from using two different techniques for representing the OD trends. In the first case, reconstructed trends are selected from an ensemble of one thousand 20th century reconstructions, representing the uncertainty in the representation of periodic climate variability. For the second case amplitudes for the CMIP5 EOFs are randomly generated from the information in the principal component time series associated with the spatial component of the EOFs, again following the method of Thompson et al. (2016).

Only combinations reducing the spread of the trends computed using the available data at each tide gauge during the 20th century are retained. In other words, after subtracting the trends associated with GIA, ocean

dynamics and the fingerprints, the standard deviation of the residual trends must be lower than the standard deviation of the tide gauge trends after subtracting the IB correction. More specifically, we seek combinations that reduce the standard deviation below a 0.2 mm/yr threshold. While this cutoff is arbitrary, subtracting the mean of the GIA solution reduces the standard deviation to 0.28 mm/yr from 0.52 mm/yr, the standard deviation of the IB-corrected tide gauge trends. As we are interested primarily in the non-GIA sea level trends, we seek combinations that reduce the standard deviation below 0.28 mm/yr. As demonstration of the sensitivity of the randomization procedure to this cutoff, we also perform a case with a standard deviation cutoff of 0.25 mm/yr that is presented in the supplementary material (supporting information Figures S2 and S3). In principle, combinations that produce the lowest standard deviations could be stated to produce the optimal 20th century trend map as they would reduce the spread of the tide gauge trends the greatest, and subsequently result in a trend map that most closely represents the actual tide gauge-measured trends. We also compute a case with a cutoff of 0.15 mm/yr using the sea level reconstruction to account for the OD component of equation (1) and find little difference compared to the case with the 0.20 mm/yr cutoff. As a final note, it is possible to perform the randomization test without requiring a cutoff. The result is a normal distribution of standard deviations in the estimated TG trends, centered roughly around 0.28 mm/yr (the standard deviation from the GIA correction alone). Since we are most interested in larger reductions in the spread, we would likely immediately subsample this distribution to keep only lower standard deviations. For this reason, we choose to apply a cutoff directly and generate more combinations that reduce the spread to the lower level defined by this cutoff.

The randomization process was repeated until 10^4 combinations are generated in both the case for the reconstruction and the case for the CMIP5 EOFs. A final correction was made to each individual trend map to account for the term GC in equation (1), representing the spatially constant contributors, such as thermal expansion, that lead to a uniform sea level rise on a global scale. The trends for the fingerprints and reconstruction (or CMIP5 dynamic trends) were subsampled at the tide gauge locations and averaged, and were then compared to the average of the actual GIA-corrected tide gauge trends. The difference of these two values was added to the total trend map. The result of this process is a trend map that when averaged globally results in an estimate that can be compared to the tide gauge bias-corrected global trend described in Thompson et al. (2016), while further agreeing with the mean of the GIA-corrected TGs trends at those specific locations. This procedure is completed for each of the 10^4 randomly generated combinations, resulting in 10^4 trend maps. Uncertainty in the individual contributors and estimated trend maps is computed using the spread of these combinations. Note that all uncertainty estimates are given as one standard deviation.

4. 20th Century Regional Sea Level Trends

The resulting 20th century regional trend maps are shown for the case using the sea level reconstruction in Figure 1a and for the case using the CMIP5 EOFs in Figure 2a. These trend maps are then subsampled at the tide gauge locations and compared to the actual GIA-corrected trends for each of the 15 gauges (Figures 1b and 2b; blue: reconstruction-modeled (1B) and ensemble-modeled (2B), red: observed GIA-corrected). Uncertainty in the 20th century trends is also estimated and shown in Figures 1c and 2c. Uncertainties are comparatively larger in the vicinity of major ice melt sources and, in Figure 2c based on CMIP5 output, around strong ocean currents. The reconstructed trend maps in Figures 1 and 2 compare favorably in many areas, although significant areas of disagreement in the open ocean are apparent. Notable areas of agreement include the increased sea level rise in the southern hemisphere, particularly in the Indian and Atlantic Oceans. Above average sea level rise is seen in both cases in large parts of the Atlantic Ocean, while lower sea level rise in the northern Indian Ocean associated with a combination of groundwater withdrawal and glacier melt is found in both instances (fingerprints shown in supporting information Figure S1). The most prominent disagreement is in the tropical Pacific, where the east-west gradient of above average to below average sea level rise is much stronger when using the sea level reconstruction. This discrepancy is similarly seen in the comparison to the actual tide gauge rates, with the CMIP5-generated trends significantly underestimating the tide gauge rate at San Diego. Likely contributing to this result, the east-west trend dipole that is visible in the tide gauge and satellite altimeter data are generally underestimated in the CMIP5 ensemble whereas the sea level reconstruction is able to accurately represent this gradient in sea level trends across the Pacific. This explanation is speculation, however, as the case using the CMIP5 also overestimates the trend in San Francisco. The difference between the subsampled rates and the actual rates is

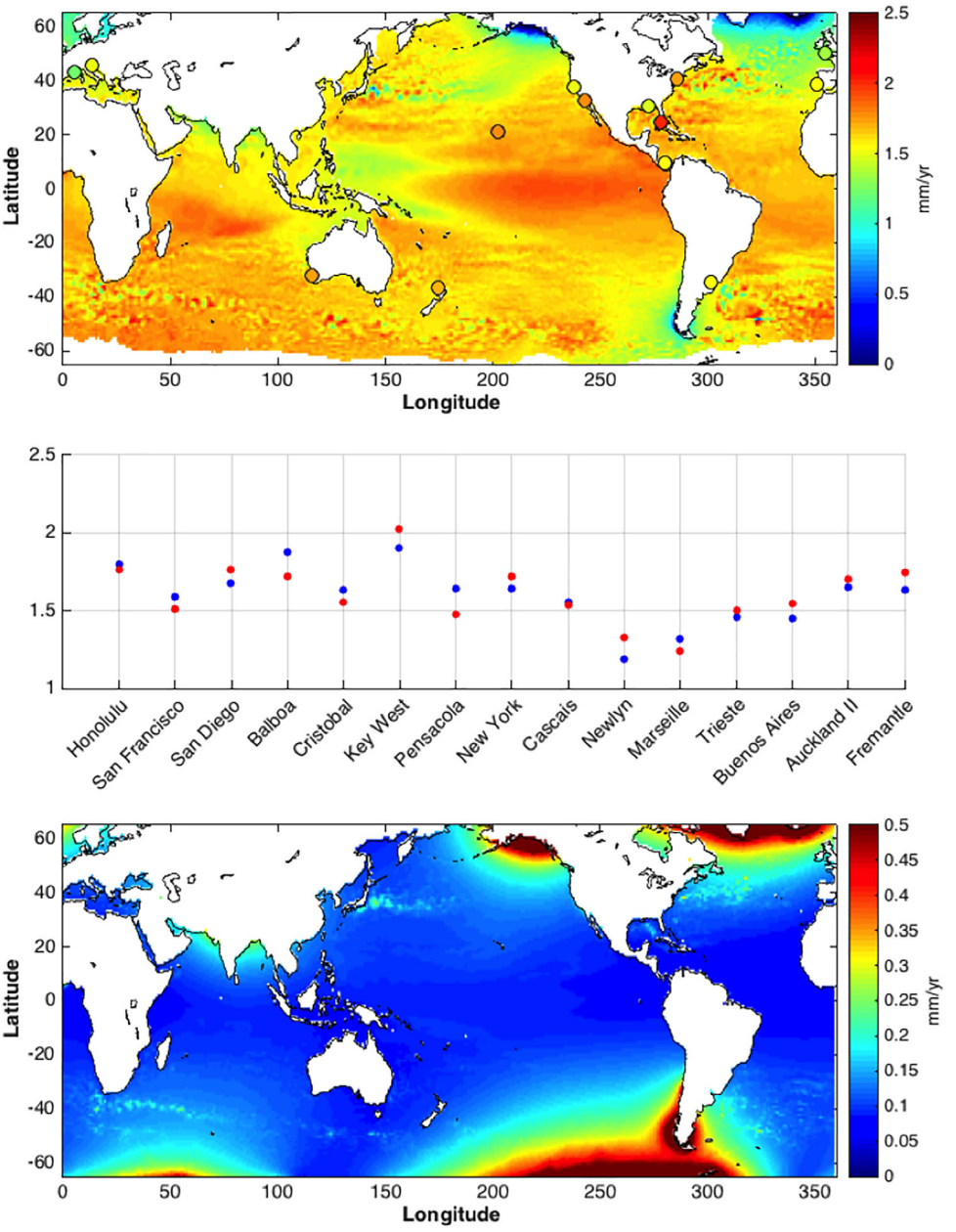

Figure 1. (a) 20th-century trend map generated using the sea level reconstruction to account for trends associated with the phasing of internal variability. (b) Comparison of the GIA-corrected trends (red) and the trends from A (blue) sub-sampled at the 15 tide-gauge locations. The mean absolute difference between the actual rates and the generated rates is 0.08 mm/yr. (c)Uncertainty in the 20th century trends.

below 0.2 mm/yr for all of the gauges in the sea level reconstruction case (mean absolute difference of 0.08 mm/yr), while 13 of the 15 gauges have trend differences below 0.2 mm/yr for the CMIP5 case (mean absolute difference of 0.11 mm/yr). While independent comparisons to other tide gauges beyond the set of 15 would add potentially add confidence to the generated trend maps, most of the other candidate tide gauges that generally meet are editing criteria are nearby to gauges that have been already been included and would thus likely lead to a favorable comparison without providing a particularly stringent test. Other tide gauges in more remote areas not covered by the set of 15 are significantly shorter than our current requirements. In the supplementary material of Thompson et al. (2016), several tide gauges were discussed in detail and the reasons for exclusion were outlined. Due to all of these issues, further comparisons could

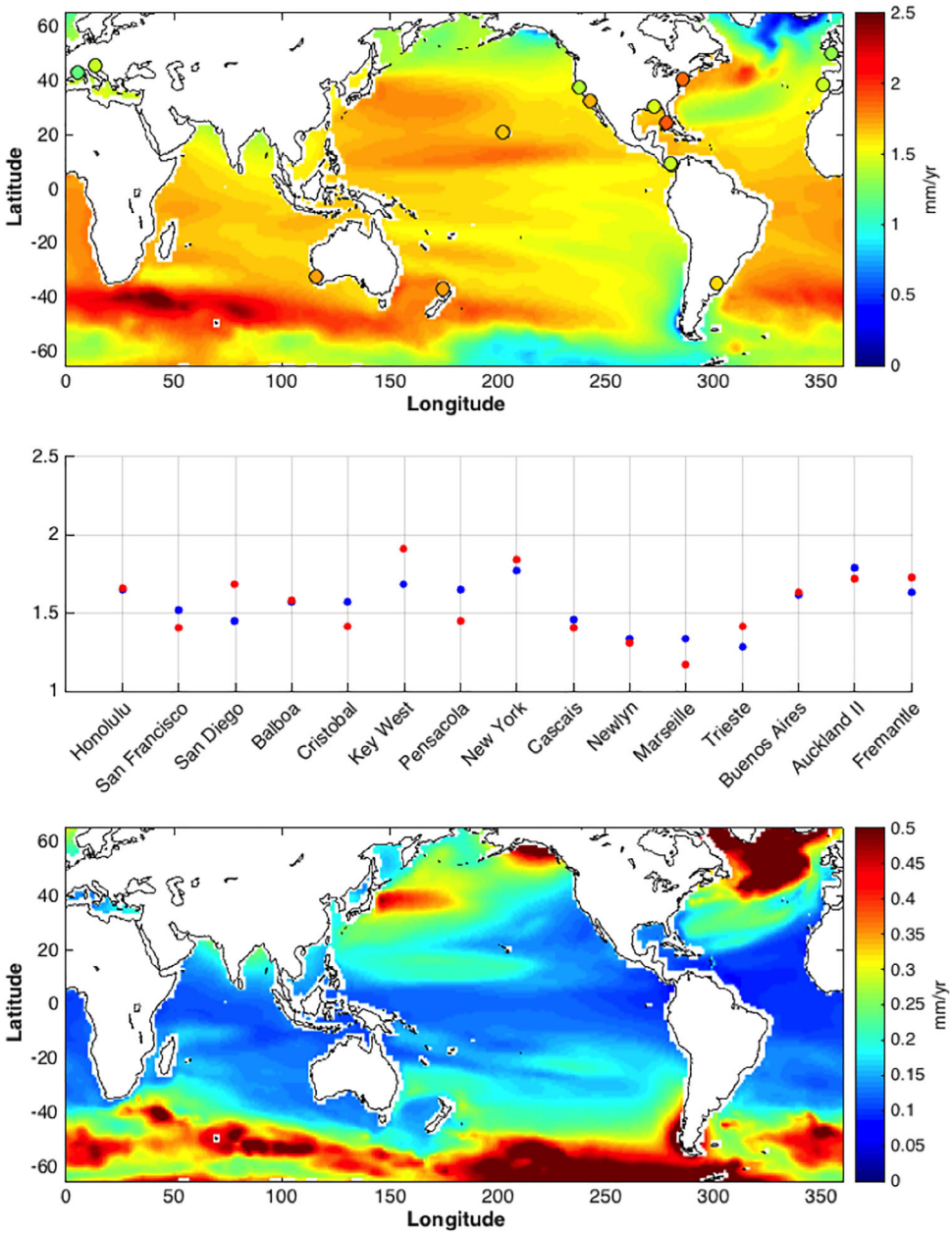

Figure 2. (a) 20th-century trend map generated using CMIP5 EOFs to account for trends associated with the phasing of internal variability. (b) Comparison of the GIA-corrected trends (red) and the trends from Figure 2a (blue) subsampled at the 15 tide-gauge locations. The mean absolute difference between the actual rates and the generated rates is 0.11 mm/yr. (c) Uncertainty in the 20th century trends.

have the purpose of providing an undue increase in the confidence in the generated trend maps, or provide a inexact test based on the construction of our approach. We do note that further work in this direction to verify the regional trend maps is warranted and should be pursued, if possible.

The GIA-corrected trends for the 15 gauges shown in Figures 1b and 2b are slightly different between the two different OD cases. This results from differences in the trends associated with GIA that are estimated in the randomization process. Figure 3 shows the expected value for the GIA rates (blue), the estimated GIA rates from the randomization process using the sea level reconstruction (red), and the estimated GIA rates from the randomization process using the CMIP5 (black). The spatial variability of the three sets is very similar, but the mean contribution of GIA in each case differs, with values of 0.24 mm/yr, 0.14 mm/yr, and

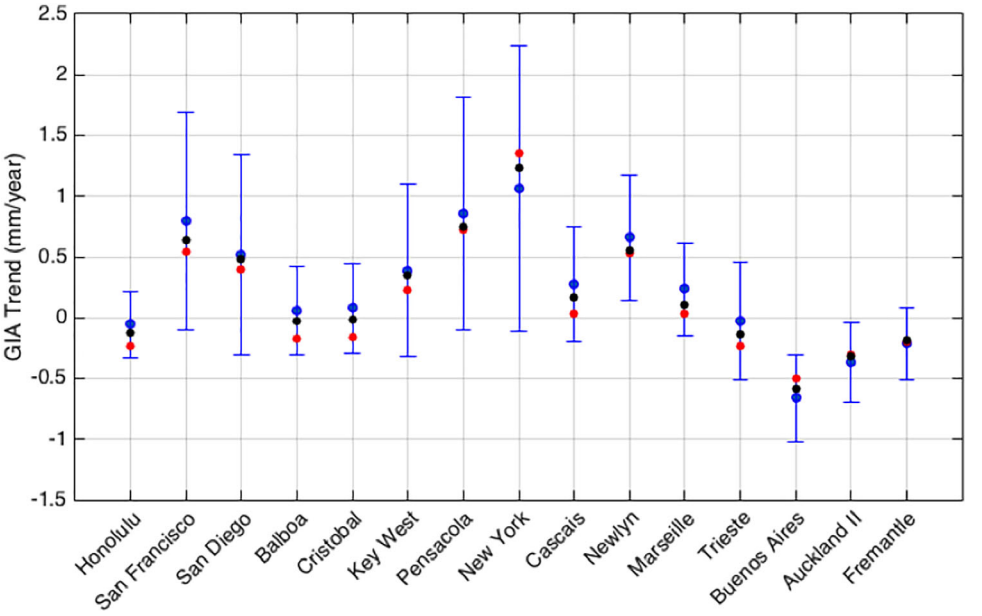

Figure 3. Trends associated with GIA for the 15 tide gauges as estimated from the randomization procedure using the reconstruction (red), and the CMIP5 EOFs (black) to account for the OD trends. The expected value for the GIA trends from the model is shown in blue, along with error bars representing the 95% confidence interval.

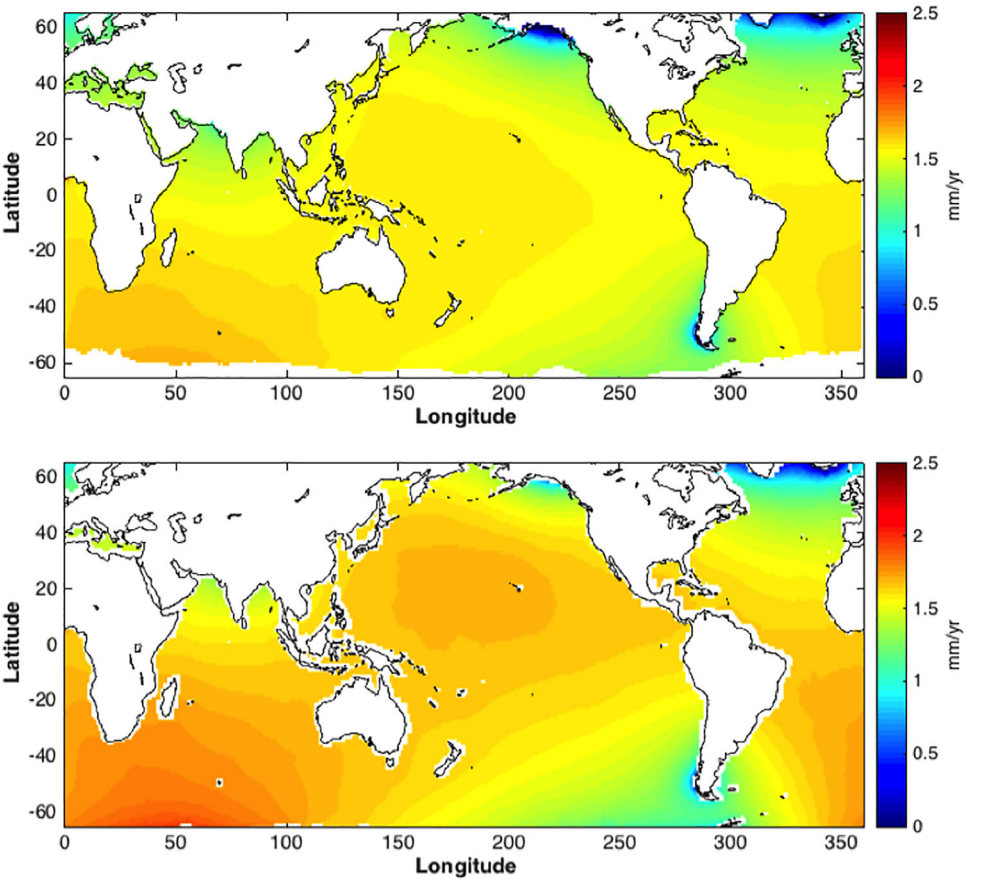

Figure 4. 20th century sea level trends associated with ice-melt, ground water pumping, water impoundment, and global mean thermal expansion for the case using the sea level reconstruction (A) and the CMIP5 EOFs (B).

Table 1
GMSL Contribution in mm/yr of Each Individual Melt Fingerprint Obtained Through the Randomization Procedure

Contribution	Recon.	CMIP5
Alaska	0.13 ± 0.09	0.08 ± 0.09
Canada	0.10 ± 0.10	0.10 ± 0.10
Asia/Alps	0.09 ± 0.09	0.13 ± 0.09
Iceland/Russia/Svalbard	0.13 ± 0.09	0.12 ± 0.09
Patagonia	0.07 ± 0.08	0.10 ± 0.08
Antarctica	0.06 ± 0.16	0.11 ± 0.15
Greenland	0.08 ± 0.12	0.13 ± 0.13
Groundwater	0.10 ± 0.06	0.05 ± 0.07
Reservoir	−0.14 ± 0.09	−0.14 ± 0.10
Total Mass	0.64 ± 0.22	0.69 ± 0.20
Global Constant	0.98 ± 0.23	0.89 ± 0.20
GMSL	1.62 ± 0.28	1.59 ± 0.40

Note. GMSL estimates are shown for both methods of accounting for the ocean dynamic signal, the sea level reconstruction and CMIP5. Uncertainty estimates represent one standard deviation as obtained by the 10^5 combinations generated through the randomization procedure.

0.19 mm/yr respectively. Contributing to these differing GIA contributions and further complicating the comparison between the two test cases is the difference between the OD trends represented by the reconstruction and CMIP5. Since the reconstruction provides data for the entire 20th century with a realistic representation of the internal variability, the trends can be computed for the specific time period covered by each individual tide gauge record. The CMIP5 EOFs are computed from the trends, with no adjustment made for differing record lengths. This would suggest that the sea level reconstruction is more appropriate for accounting for the OD component given the record lengths of the 15 gauges used here, although this point is difficult to verify.

By removing the spatial trend variability associated with the term OD in equation (1) as represented by the reconstruction and CMIP5 EOFs, the spatial pattern of long-term sea level rise associated with mass redistribution (terms IM, GW, WI) can be isolated. Furthermore, by forcing the trends at the tide gauge locations obtained from the maps in Figures 1 and 2 to have the same mean trend as the actual GIA-corrected trends, we can include the trend represented by GC in equation (1) that includes the contribution from global mean thermal expansion. The resulting trends arising from the combination ice melt and this globally constant trend are shown in Figure 4. There is considerable agreement between the two generated trend maps. Higher than average sea level rise is found off the U.S. west coast and in the southern Indian and Atlantic Oceans, with lower than average sea level rise in the south Pacific and northern parts of the Atlantic, Indian and Pacific Oceans.

While estimating regional sea level rise, we can estimate the contribution of each term in equation (1) to global mean sea level rise during the 20th century (Table 1). The fingerprints used are spatially correlated and the uncertainty range is large for most contributors so we avoid over-analyzing the global contribution of any individual fingerprint. Combined, however, mass redistribution (includes ice melt, groundwater withdrawal and water impoundment) contributes 0.64 +/− 0.22 mm/yr and 0.69 +/− 0.20 mm/yr in the cases of the reconstruction and the CMIP5, respectively, within the ranges described by other studies (e.g., Church et al., 2013; Mitrovica et al., 2006; Vaughan et al., 2013). Ensuring the final trend map has the same mean at the subsampled tide gauge locations as the GIA-corrected tide gauge trends (using the GIA corrections shown in Figure 3), the GC contributes a further 0.98 +/− 0.23 mm/yr and 0.89 +/− 0.20 mm/yr over the 20th century for the reconstruction and CMIP5, respectively. This leads to a final estimate of global mean sea level rise in the 20th century of 1.63 +/− 0.33 mm/yr and 1.59 +/− 0.40 mm/yr. Finally, with the mean of the GIA-corrected tide gauge trends 1.55 mm/yr and 1.50 mm/yr for the two cases, it is found that the tide gauge locations considered here under-sampled the global rate by 0.08 mm/yr and 0.09 mm/yr, respectively. This is in agreement with the estimate of Thompson et al. (2016), with the addition of taking into account the additional contributions of groundwater withdrawal and water impoundment which approximately cancel out in their contribution to GMSL. This should not be taken as a validation of the results in Thompson et al. (2016) given the similar approach and the same underlying data that have been used. Instead, it is used a check on the modified technique presented here, arriving at an expected similar result to that previously presented.

5. Discussion and Conclusion

Assessing the absolute quality and accuracy of the reconstructed trend maps presented here is difficult due to a lack of additional independent data. While it might initially seem worthwhile to use other tide gauges as an independent verification of the generated trend maps, such comparisons are a challenge, specifically because few tide gauges span the complete record considered here (1901–2000). The trend associated with ocean dynamics can and does vary dramatically depending on the start and end date of the record. As such, the 20th century trend patterns here will not necessarily be representative of the trend at a tide gauge with a shorter record. While the sea level reconstruction could be used to account for this problem, the

presence of non-GIA vertical land motion and uncertainty in GIA corrections prohibits the use of many of long tide gauge records for the purposes of comparison. Several recent studies have used GPS-measured trends at or near the tide gauges to remove trends associated with the relative motion of land (e.g., Dangendorf et al., 2017; Hamlington et al. 2016a; Wöppelmann & Marcos, 2016), but in the case of our 15 gauges, questions remain as to how representative these GPS rates are. Our attempts to correct 20th century rates from long tide gauge records using GPS for the vertical land motion component of relative sea level rise (results not shown) demonstrated that corrections derived directly from GPS measurements for the gauges considered here lead to a large increase in the spread amongst the estimated trends. The increase in spread implies that the GPS-based corrections, in this specific case using the 15 gauges, is perhaps introducing error into the calculations. It should be noted that while efforts have been made to select tide gauges relatively unaffected by non-GIA vertical land motion, any remaining and thus uncorrected vertical land motion will impact the resulting trend maps. As an example, there is recently published evidence of non-GIA vertical land motion at the Fremantle tide gauge that was used in this study (Featherstone et al., 2015).

With regards to the correction for GIA relative sea level rates, this study does highlight a large source of uncertainty in the 20th century estimate of global mean sea level that has been discussed in previous studies (e.g., Jevrejeva et al., 2014). The results presented here suggest that this could lead to an underestimate of the uncertainty in the 20th century global rate, although this again may be specific to the set of tide gauges used here. Using the reconstruction, the randomization procedure returns a 95% confidence interval on the mean contribution of GIA at the tide gauge locations ranging from -0.01 mm/yr to 0.29 mm/yr. A higher estimate of the mean in the GIA-related trends at the tide gauge would simply serve to lower the estimate of the trend in global mean sea level provided in Table 1 without dramatically altering the spatial variability in the trends maps shown in Figures 1, 2, and 4. Specifically, the estimate of GC would change with adjustments in the mean of the GIA-related trends. A higher GMSL contribution from GIA would lower the estimate of GC, while a lower contribution would increase the estimate of GC. When compared to the results of Thompson et al. (2016), incorporating uncertainty in the GIA correction does lead to an increase of the uncertainty in the estimate of the 20th century trend in GMSL. In summary, improving the estimates of how GIA impacts sea level measurements taken by tide gauges is critical to our understanding of 20th century sea level.

It is worth noting that the GMSL trend is larger than other recently published estimates covering a similar time period (e.g., Dangendorf et al., 2017; Hay et al., 2015). Based on their location, the 15 gauges selected here underestimate the positive contribution of 5 of the 7 ice fingerprints along with the contribution from GW, and overestimate the negative contribution from WI. In order for the estimate of GMSL rise during the 20th century to be lower than provided here, we can consider the following possible situations: 1) the 15 tide gauges are on average significantly impacted by non-GIA subsidence; 2) the average GIA contribution is significantly underestimated; 3) the distributions from which the amplitudes of the fingerprints are drawn are incorrect; 4) there is a negative global trend associated with OD that is not being accounted for; and 5) a relatively large contribution to regional and global sea level is unaccounted for. We consider (4) and (5) to be unlikely, and checking and accounting for (3) is beyond the scope of an individual paper. It is possible that (1) and (2) could lead to an overestimate of the trend in GMSL and subsequently GC, and require further investigation in the future. Also, while it would not impact the GMSL trend estimate obtained here, an increase in the estimated GMSL rise resulting from mass redistribution fingerprints would lead to a decrease in the contribution associated with GC.

Even with the described uncertainties and caveats, this study represents a comprehensive attempt to understand regional sea level trend variability during the 20th century applying the current method. We have sought to simplify the process of constructing a map of regional sea level rise by reducing uncertainty and complexity wherever possible and leveraging the best available information about the spatial variability in long-term sea level trends. While the randomization procedure and use of a small subset of available tide gauge records has limitations, the methods and results presented here represent an attempt to transparently parse the leading-order contributions to regional 20th century sea level trends. We view this study as the foundation for a more formal approach to be pursued in future studies. On a fundamental level, the generated spatial patterns of 20th century sea level rise meet the essential requirement of agreeing with the highest-quality and longest tide gauge records. While seemingly a very basic requirement, this criterion has

not been prioritized by previously published studies. Beyond this, this study yields important information for planning purposes. On century timescales, considerable spatial variability in regional trends can occur, spanning a range of several mm/yr. The spatial variability of trends is essential to understand when planning for future sea level rise at a particular location. This study also emphasizes the need to account for natural, periodic variability that can serve to obscure the sea level trends associated with global warming. In particular, Figure 4 shows the regional trend pattern most closely linked to anthropogenic forcing and thus may be indicative of the regional variability of sea level rise in the future. It is these trends that are of particular interest for long-term planning as they arise from contributors that are secular in nature and may be expected to persist into the future. From this figure, the western Pacific, and southern Indian and Atlantic Oceans would be expected to have sea level trends greater than the global mean. It is important to note that the trends represented here do not take into account changes in reference due to GIA or non-GIA vertical land motion. For example, the lower trends off the eastern United States shown in Figure 4 are significantly higher when including the impact of GIA. The goal of this study, however, is on isolating the trends most closely linked to anthropogenic forcing and obtaining a better understanding of how these trends vary regionally.

Acknowledgments

The satellite altimetry data are publicly available through the Archiving, Validation and Interpretation of Satellite Oceanographic (AVISO) website (http://www.aviso.oceanobs.com/en/data/products/sea-surface-height-products/). The tide gauge data is available from the Permament Service for Mean Sea Level (PSMSL; www.psmsl.org/data/). B.D.H. and A.B. acknowledge support from NASA New Investigator Program NNX16AH56G. P.R.T acknowledges support from the NOAA Climate Program Office in support of the University of Hawaii Sea Level Center. C.G.P. acknowledges support from the National Science Foundation, award 1558966.

References

Adhikari, S., Ivins, E. R., & Larour, E. (2016). ISSM-SESAW v1.0: Mesh-based computation of gravitationally consistent sea-level and geodetic signatures caused by cryosphere and climate driven mass change, *Geoscientific Model Development*, 9, 1087–1109.

Boening, C.,J. K., Willis, F. W., Landerer, R. S., Nerem, J. & Fasullo, (2012). The 2011 La Niña: So Strong, the Oceans Fell. *Geophysical Research Letters*, *39*, L19602. https://doi.org/10.1029/2012GL053055

Calafat, F. M., Chambers, D. P., & Tsimplis, M. N. (2014). On the ability of global sea level reconstructions to determine trends and variability. *Journal of Geophysical Research: Oceans*, *119*, 1572–1592. https://doi.org/10.1002/2013JC009298

Caron, L., Métivier, L., Greff-Lefftz, M., Fleitout, L., & Rouby, H. (2017). Inverting Glacial Isostatic Adjustment signal using Bayesian framework and two linearly relaxing rheologies. *Geophysical Journal International*, *209*(2), 1126–1147.

Caron, L., Ivins, E. R., Larour, E., Adhikari, S., Nilsson, J., & Blewitt, G. (2018). GIA model statistics for GRACE hydrology, cryosphere, and ocean science. *Geophysical Research Letters*, 45.

Cazenave, A., Henry, O., Munier, S., Delcroix, T., Gordon, A. L., Meyssignac, B., et al. (2012). Estimating ENSO influence on the global mean sea level, 1993–2010. *Marine Geodesy*, *35*, 82–97.

Church, J. A., Clark, P. U., Cazenave, A., Gregory, J. M., Jevrejeva, S., Levermann, A., et al. (2013). Sea level change. In Stocker, T. F., et al., *Climate change 2013: The physical science basis. Contribution of working group I to the fifth assessment report of the intergovernmental panel on climate change*. Cambridge, UK and New York, NY: Cambridge University Press.

Church, J. A., White, N. J., Coleman, R., Lambeck, K., & Mitrovica, J. X. (2004). Estimates of the regional distribution of sea level rise over the 1950–2000 period. *Journal of Climate*, *17*, 2609–2625.

Church, J. A., & White, N. J. (2006). A 20th century acceleration in global sea level rise. *Geophysical Research Letters*, *36*, L01602, https://doi.org/10.1029/2005GL024826

Church, J. A., & White, N. J. (2011). Sea-level rise from the late 19th to the early 21st century. *Surveys in Geophysics*, *32*(4), 585–602.

Dangendorf, S., Marcos, M., Wöppelmann, G., Conrad, C. P., Frederikse, T., & Riva, R. (2017). Reassessment of 20th century global mean sea level rise. *Proceedings of National Academy of Sciences of the United States of America*, *114*(23), 5946–5951.

Fasullo, J. T., Boening, C., Landerer, F. W., & Nerem, R. S. (2013). Australia's Unique Influence on Global Sea Level in 2010–2011. *Geophysical Research Letters*, *40*, 4368–4373. https://doi.org/10.1002/grl.50834

Featherstone, W. E., Penna, N. T., Filmer, M. S., & Williams, S. D. P. (2015). Nonlinear subsidence at Fremantle, a long-recording tide gauge in the Southern Hemisphere. *Journal of Geophysical Research: Oceans*, *120*, 7004–7014. https://doi.org/10.1002/2015JC011295

Gregory, J. M., White, N. J., Church, J. A., Bierkens, M. F. P., Box, J. E., van den Broeke, M. R., et al. (2013). Twentieth-century global-mean sea level rise: Is the whole greater than the sum of the parts? *Journal of Climate*, *26*(13), 4476–4499.

Hamlington, B. D., Leben, R. R., Nerem, R. S., Han, W., & Kim, K.-Y. (2011). Reconstruction sea level using cyclostationary empirical orthogonal functions. *Journal of Geophysical Research*, *116*, C12015. https://doi.org/10.1029/2011JC007529

Hamlington, B. D., Leben, R. R., & Kim, K.-Y. (2012). Improving sea level reconstructions using non-sea level measurements. *Journal of Geophysical Research*, *117*, C10025. https://doi.org/10.1029/2012JC008277

Hamlington, B. D., Thompson, P., Hammond, W. C., Blewitt, G., & Ray, R. D. (2016a). Assessing the impact of vertical land motion on twentieth century global mean sea level estimates. *Journal of Geophysical Research: Oceans*, *121*, 4980–4993. https://doi.org/10.1002/2016JC011747

Hamlington, B. D., Cheon, S. H., Thompson, P. R., Merrifield, M. A., Nerem, R. S., Leben, R. R., & Kim, K.-Y. (2016b). An ongoing shift in Pacific Ocean sea level. *Journal of Geophysical Research: Oceans*, *121*, 5084–5097. https://doi.org/10.1002/2016JC011815

Hay, C. C., Morrow, E., Kopp, R. E., & Mitrovica, J. X. (2015). Probabilistic reanalysis of twentieth-century sea level rise. *Nature*, *517*, 481–484.

Hay, C. C., Morrow, E., Kopp, R. E., & Mitrovica, J. X. (2017). On the robustness of Bayesian fingerprinting estimates of global sea level change. *Journal of Climate*, *30*(8), 3025–3038.

Huang, B., Thorne, P., Smith, T., Liu, W., Lawrimore, J., Banzon, V., et al. (2015). Further exploring and quantifying uncertainties for extended reconstructed sea surface temperature (ERSST) version 4 (v4). *Journal of Climate*, *29*, 3119–3142.

Huybrechts, P., Goelzer, H., Janssens, I., Driesschaert, E., Fichefet, T., Goosse, H., & Loutre, M. F. (2011). Response of the Greenland and Antarctic ice sheets to multi-millennial greenhouse warming in the Earth system model of intermediate complexity LOVECLIM. *Surveys in Geophysics*, *32*(4–5), 397–416.

Ivins, E. R., & James, T. S. (2004). Bedrock response to Llanquihue Holocene and present-day glaciation in southernmost South America. *Geophysical Research Letters*, *31*, L24613. https://doi.org/10.1029/2004GL021500

Ivins, E. R., James, T. S., Wahr, J., Schrama, E. J. O., Landerer, F. W., & Simon, K. M. (2013). Antarctic contribution to sea-level rise observed by GRACE with improved GIA correction. *Journal of Geophysical Research: Solid Earth*, *118*, 3126–3141, . https://doi.org/10.1002/jgrb.50208

Jevrejeva, S., Moore, J. C., Grinsted, A., Matthews, A. P., & Spada, G. (2014). Trends and Acceleration in Global and Regional Sea Levels since 1807. *Global and Planetary Change*, *113*, 11–22.

Lambeck, K., Purcell, A., Zhao, J., & Svensson, N. O. (2010). The Scandinavian ice sheet: From MIS 4 to the end of the Last Glacial Maximum. *Boreas*, *39*(2), 410–435.

Lambeck, K., Rouby, H., Purcell, A., Sun, Y., & Sambridge, M. (2014). Sea level and global ice volumes from the Last Glacial Maximum to the Holocene. *Proceedings of the National Academy of Sciences of the United States of America*, *111*(43), 15296–15303.

Lehner, B., Reidy Liermann, C., Revenga, C., Vörösmarty, C., Fekete, B., Crouzet, P., et al. (2011). High-Resolution Mapping of the World's Reservoirs and Dams for Sustainable River-Flow Management. *Frontiers in Ecology and the Environment*, *9*(9), 494–502.

Milne, G. A., Long, A. J., & Bassett, S. E. (2005). Modelling Holocene relative sea-level observations from the Caribbean and South America. *Quaternary Science Reviews*, *24*(10), 1183–1202.

Mitrovica, J. X., Wahr, J., Matsuyama, I., Paulson, A., & Tamisiea, M. E. (2006). Reanalysis of ancient eclipse, astronomic and geodetic data: A possible route to resolving the enigma of global sea-level rise. *Earth and Planetary Science Letters*, *243*(3–4), 390–399.

Piecuch, C. G., Thompson, P. R., & Donohue, K. A. (2016). Air pressure effects on sea level changes during the twentieth century. *Journal of Geophysical Research: Oceans*, *121*, 7917–7930. https://doi.org/10.1002/2016JC012131

Ray, R., & Douglas, B. (2011). Experiments in reconstructing twentieth-century sea levels. *Progress in Oceanography*, *91*, 496–515.

Santamaría-Gómez, A., Gravelle, M., Collilieux, X., Guichard, M., Míguez, B. M., Tiphaneau, P., & Wöppelmann, G. (2012). Mitigating the effects of vertical land motion in tide gauge records using a state-of-the-art GPS velocity field. *Global and Planetary Change*, *98*, 6–17.

Thompson, P. R., Hamlington, B. D., Landerer, F. W., & Adhikari, S. (2016). Are long tide gauge records in the wrong place to measure global mean sea level rise? *Geophysical Research Letters*, *43*, 10403–10411. https://doi.org/10.1002/2016GL070552

Vaughan, D. G., Comiso, J. C., Allison, I., Carrasco, J., Kaser, G., Kwok, R., et al. (2013). Observations: Cryosphere. In Stocker, T. F., et al. (Eds.), *Climate change 2013: The physical science basis. Contribution of working group I to the fifth assessment report of the intergovernmental panel on climate change*. Cambridge, UK and New York, NY: Cambridge University Press.

Wada, Y., vanBeek, L. P. H., Sperna Weiland, F. C., Chao, B. F., Wu, Y.-H., & Bierkens, M. F. P. (2012). Past and future contribution of global groundwater depletion to sea-level rise. *Geophysical Research Letters*, *39*, L09402. https://doi.org/10.1029/2012GL051230

Wenzel, M., & Schröter, J. (2014). Global and regional sea level change during the 20th century. *Journal of Geophysical Research: Oceans*, *119*, 7493–7508. https://doi.org/10.1002/2014JC009900

Wöppelmann, G., & Marcos, M. (2016). Vertical land motion as a key to understanding sea level change and variability. *Reviews of Geophysics*, *54*, 64–92. https://doi.org/10.1002/2015RG000502